Evolutionary analysis and molecular dissection of caveola biogenesis

Matthew Kirkham[1,2], Susan J. Nixon[1,2,*], Mark T. Howes[1,2,*], Laurent Abi-Rached[3,*], Diane E. Wakeham[4], Michael Hanzal-Bayer[1], Charles Ferguson[1,2], Michelle M. Hill[1], Manuel Fernandez-Rojo[1,2], Deborah A. Brown[5], John F. Hancock[1], Frances M. Brodsky[4] and Robert G. Parton[1,2,‡]

[1]Institute for Molecular Bioscience and [2]Centre for Microscopy and Microanalysis, University of Queensland, Queensland 4072, Brisbane, Australia
[3]Department of Structural Biology, Stanford University School of Medicine, Stanford, CA 94305, USA
[4]The G.W. Hooper Foundation, Departments of Biopharmaceutical Sciences, Pharmaceutical Chemistry and Microbiology and Immunology, University of California, San Francisco, CA 94143-0552, USA
[5]Department of Biochemistry and Cell Biology, Stony Brook University, Stony Brook, NY, USA,
*These authors contributed equally to this work
‡Author for correspondence (e-mail: R.Parton@imb.uq.edu.au)

Accepted 7 April 2008
Journal of Cell Science 121, 2075-2086 Published by The Company of Biologists 2008
doi:10.1242/jcs.024588

Summary

Caveolae are an abundant feature of mammalian cells. Integral membrane proteins called caveolins drive the formation of caveolae but the precise mechanisms underlying caveola formation, and the origin of caveolae and caveolins during evolution, are unknown. Systematic evolutionary analysis shows conservation of genes encoding caveolins in metazoans. We provide evidence for extensive and ancient, local and genomic gene duplication, and classify distinct caveolin gene families. Vertebrate caveolin-1 and caveolin-3 isoforms, as well as an invertebrate (*Apis mellifera*, honeybee) caveolin, all form morphologically identical caveolae in caveolin-1-null mouse cells, demonstrating that caveola formation is a conserved feature of evolutionarily distant caveolins. However, coexpression of flotillin-1 and flotillin-2 did not cause caveola biogenesis in this system. In contrast to the other tested caveolins, *C. elegans* caveolin is efficiently transported to the plasma membrane but does not generate caveolae, providing evidence of diversity of function in the caveolin gene family. Using *C. elegans* caveolin as a template to generate hybrid caveolin constructs we now define domains of caveolin required for caveolae biogenesis. These studies lead to a model for caveola formation and novel insights into the evolution of caveolin function.

Supplementary material available online at
http://jcs.biologists.org/cgi/content/full/121/12/2075/DC1

Key words: Biogenesis, Caveolae, Caveolin, Evolution

Introduction

Caveolae, flask-shaped invaginations of the plasma membrane, are a striking feature of many mammalian cells. Caveolae are defined by their morphology and by the presence of integral membrane proteins, called caveolins (Parton et al., 2006). Caveolins and caveolae have been linked to diseases such as cancer (Hayashi et al., 2001; Koleske et al., 1995) and muscular dystrophy (Galbiati et al., 1999; Minetti et al., 1998; Woodman et al., 2004), highlighting the importance of understanding the relationship between caveolae morphology and their functions. Caveolins are fundamental to caveola formation in mammalian cells (Parton et al., 2006). Caveolae can be generated de novo by the transient expression of caveolin-1 (Cav1) (Fra et al., 1995) or the muscle specific isoform caveolin-3 (Cav3) (Capozza et al., 2005), and are regulated by a cytoplasmic protein PTRF (polymerase I and transcript release factor)-Cavin (Hill et al., 2008; Liu and Pilch, 2008). Recently the coexpression of flotillin-1 (also known as FLOT1, reggie-2) and flotillin-2 (also known as FLOT2, reggie-1) has also been reported to induce the formation of caveola-like structures (Frick et al., 2007). Caveolin-2 (Cav2) has an overlapping expression pattern with Cav1 in most tissues (Scherer et al., 1996) and when coexpressed, is localised to caveolae. When Cav2 is expressed without Cav1 or Cav3 it is localised to the Golgi complex (Mora et al., 1999). This suggests Cav2 has a regulatory role in caveola formation and dynamics (Sowa et al., 2003). Cav2 may have an additional role distinct from caveolae formation, as shown by the fact that Cav2-null mice form caveolae, but display evidence of severe pulmonary dysfunction (Razani et al., 2002b). Cav1 binds directly to cholesterol (Murata et al., 1995) and cholesterol is required for caveola formation or stability, because cholesterol depletion disrupts caveolar structure (Rothberg et al., 1992). However, the molecular details of caveola formation induced through caveolin-membrane interactions are still unknown.

All caveolin family members are predicted to have a 33 amino acid intramembrane domain with both N- and C-termini facing the cytoplasm (Parton et al., 2006). The C-terminus is palmitoylated during transit through the secretory pathway (Dietzen et al., 1995). Cav1 and Cav3 can form high-molecular-weight complexes through homo- and hetero-oligomerisation (Monier et al., 1995; Tang et al., 1996) that become enriched in low-density fractions following density gradient centrifugation after treatment with specific detergents (Kurzchalia et al., 1992). A large number of deletion, truncation and amino-acid substitution mutants of Cav1 and Cav3 that are retained within the Golgi complex also have an impaired ability to oligomerise and/or become detergent insoluble (Luetterforst et al., 1999; Machleidt et al., 2000; Ren et al., 2004). These include a number of Cav3 mutations that are associated with muscle diseases (Galbiati et al., 1999; Woodman et al., 2004). This has led to the hypothesis

that Cav1 or Cav3 must adopt the correct protein conformation to exit the Golgi complex and that this conformation is very sensitive to alterations in the amino acid sequence (Ren et al., 2004).

Examination of systems from across the diversity of eukaryotes has provided important insights into numerous aspects of membrane traffic. Sequence homology searches have suggested that caveolins appeared relatively late in eukaryotic evolution and are specific to the metazoan (vertebrate and invertebrate animal) branch of opisthokonta but absent from the fungi (yeast) branch, as well as from plants and non-metazoan parasites (Field et al., 2007). Among metazoans, caveolins are evolutionarily conserved from humans to nematodes (Spisni et al., 2005; Tang et al., 1997) but apparently absent from *Drosophila melanogaster*. It is also unclear when caveolins acquired the property of caveola formation during metazoan evolution. Caveolin function has been studied in three non-mammalian systems. In *Danio rerio* (zebrafish), both caveolins and putative caveolae structures have been described (Nixon et al., 2005). In the adult *Xenopus laevis*, caveolin expression has been detected in lung, muscle and fat tissues, similar to its expression pattern in mammals (Razani et al., 2002a). In *C. elegans* there are two isoforms of caveolin but only *C. elegans* Cav1 (*Ce*Cav1) has been studied. *Ce*Cav1 was not ubiquitously expressed in the adult hermaphrodite nematode, but was present within the gonad arm (Scheel et al., 1999) and both neurons and body wall muscles, where it was suggested to have a role at the neuromuscular junction (Parker et al., 2007). *Ce*Cav1 was also localised to the plasma membrane of cells within the early embryo where it was endocytosed in a clathrin-dependent manner (Sato et al., 2006). However, no study has directly addressed whether *Ce*Cav1 can form caveolae.

We have established a system to analyse de novo formation of caveolae in mammalian cells lacking caveolae and in combination with phylogenetic analysis we have studied the evolution of caveolins and caveolae. We show that the ability of caveolin to form caveolae has not been conserved in *C. elegans* but has been conserved in another branch of invertebrate caveolins (i.e. that of *Apis mellifera*, honeybee). Furthermore, genomic comparison of caveolins showed a pattern of gene duplication and loss in both the vertebrate and invertebrate lineages. *Ce*Cav1 was used as a scaffold to create hybrid constructs between different caveolins in order to analyse the importance of specific domains of mammalian caveolin in caveola formation. In combination with a range of truncation and point mutants we have identified previously uncharacterised domains in mammalian Cav1 that are fundamental for caveola formation. We also demonstrated that, in cells that lack Cav1, flotillin-1 and flotillin-2 could not form caveola-like structures. These results lead to new insights into the functional evolution of caveolins and the development of a new model for caveola formation.

Results

Evolutionary analysis of caveolins and caveolae formation in metazoans

Cav1 and Cav3 are essential for caveola formation in mammalian cells but the role of caveolins in other eukaryotes is less clear. To increase the understanding of caveolin biology, we performed an extensive database search for caveolin sequences and identified new sequences in expressed sequence tag (EST) and genomic databases (supplementary material Table S1). The caveolin sequences we gathered in these searches all belong to metazoans and none were observed in the genome of the choanoflagellate *Monosiga brevicollis*, an observation consistent with the prediction that caveola formation arose in the animal lineage (Field et al., 2007). A considerable degree of conservation was observed among all sequences analysed (supplementary material Fig. S1), with the most divergent regions in the distal N- and C-termini.

To establish the pattern of diversification of the caveolins in metazoans we performed a phylogenetic analysis using the most conserved region of caveolins – equivalent to amino acids R54 to P158 in human CAV1 (*Hs*Cav1) – approximately half of the protein (supplementary material Fig. S1). Four different phylogenetic methods were used in this study (Bayesian interference, maximum-likelihood (ML), neighbour-joining (NJ), parsimony) and they all indicate that two ancient groups of caveolin can be distinguished: the 'classical' caveolin group, which includes all known vertebrate caveolins, and a 'caveolin-like' group which includes a demosponge, an annelide and three chordate sequences (Fig. 1). In the classical caveolin group the vertebrate sequences fall into three well-supported groupings, a Cav1-Cav3 group, a Cav2-Cav2-related-sequences (Cav2R) group and the CavY clade. The latter group is the only of these three groups to include non-vertebrate sequences and comprises two tunicate sequences (CavY minimum group, Fig. 1).

The relationships of the protostomian (worms, arthropods and molluscs) and non-bilaterian (sea anemones and the placozoan *Trichoplax*) caveolin sequences with the three groups of vertebrate sequences are not fully resolved. Indeed, whereas protostome sequences form three groups (G1-G3, Fig. 1) only one (G1) is related to vertebrate sequences, a relationship supported by two of the four phylogenetic methods ('CavY extended'; Fig. 1). Interestingly, the NJ analysis suggested that G1 and G3 form a single group (interior branch test support: 98). To test whether the two nematode sequences forming the G3 group are divergent members of the G1 group and whether this divergence contributes to the partial support for the G1 and 'CavY extended' groups, we repeated the phylogenetic analysis without these two sequences. The new analysis shows an increased support for the G1 and CavY extended groups (Fig. 1), reinforcing the possibility that the G1 and 'CavY minimum' groups are related. If so, the duplication between CavY and the other two vertebrate groups (Cav1-Cav3, Cav2-Cav2R) preceded the protostome-deuterostome split. Such an ancient split is also seen for the two main protostome groups because G1 and G2 both contain arthropod sequences, but the arthropod G2 sequences are more related to the nematode G2 sequences than to the arthropod G1 sequences. This indicates that the G1-G2 separation took place before the nematode-arthropod split. To account for the uncertainty in the relationships between the vertebrate and non-vertebrate sequences we have used suffixes (-a, -b, etc.) to name the duplicated caveolin sequences in non-vertebrates. In view of this new analysis it is misleading to describe *C. elegans* caveolins as Cav1 or Cav2; therefore, *Ce*Cav1, for example, will here be referred to as *Ce*Cav-a (*C. elegans* Cav-a).

The phylogenetic analysis suggests that the duplications between Cav1 and Cav3 and between Cav2 and Cav2R both occurred in vertebrates. In human, pufferfish and *Xenopus tropicalis* genomes, *Cav1* and *Cav2* are located next to each other, whereas *Cav3* is on another chromosome (Fig. 2A). The presence of a *Cav2R* gene in bony fishes and frogs next to the *Cav3* orthologue suggests that the Cav1-Cav2 and the Cav3-Cav2R genomic segments originate from a single en-bloc duplication in a vertebrate ancestor. This then raises the question of when the duplication between the ancestor of *Cav1* and *Cav3* (*CavX*) and the ancestor of *Cav2* and *Cav2R* (*CavZ*)

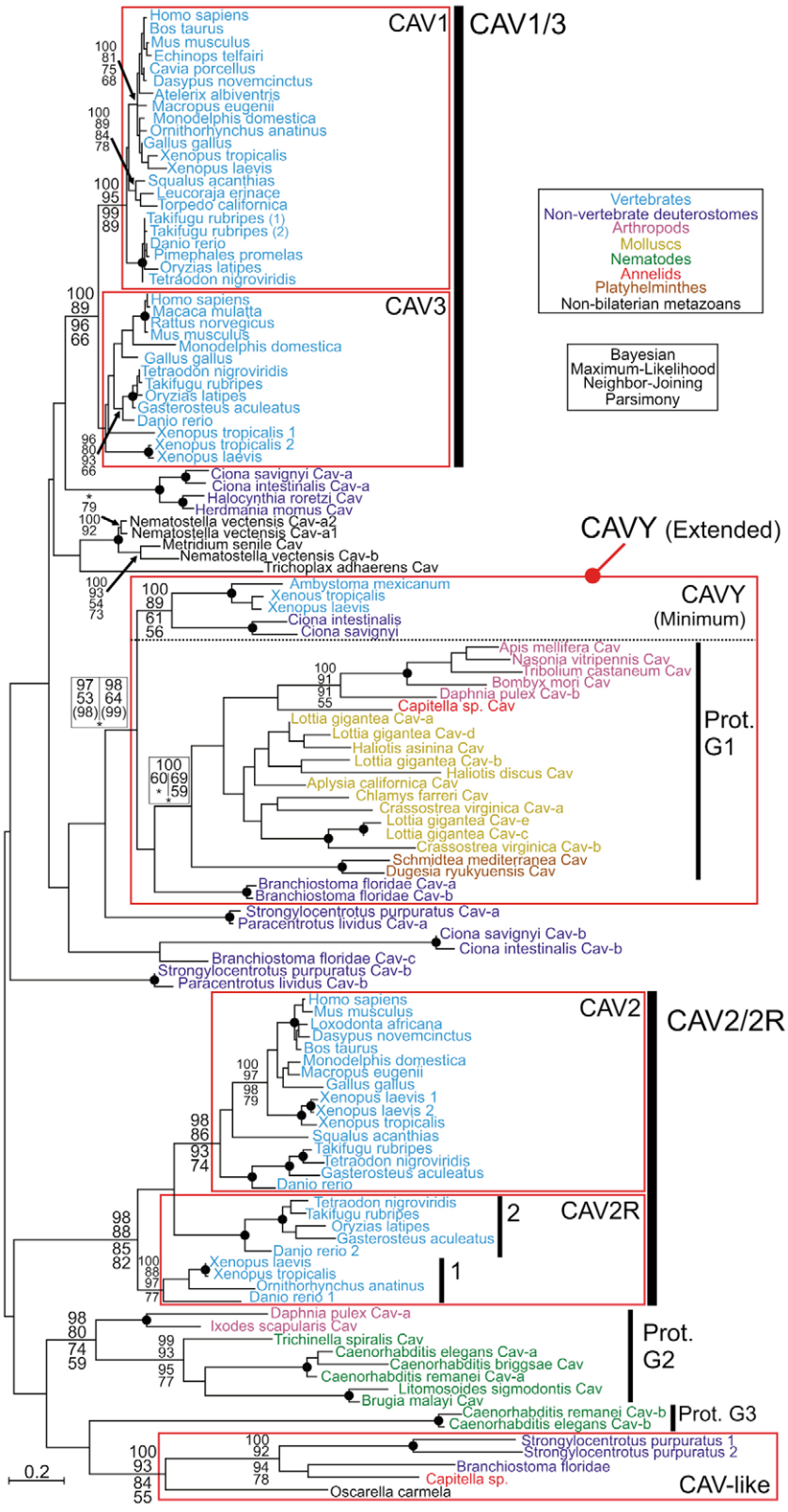

Fig. 1. Evolutionary conservation of caveolins. Caveolin phylogeny. Phylogenetic analyses were performed with Bayesian interference, ML, NJ and parsimony methods from the alignment of caveolin sequences to R54 to P158 in *Hs*Cav1 to P158. The ML tree topology was used for the display (with a midpoint rooting) and the node support is given in the following order (from top to bottom): Bayesian (posterior probability, PP), ML, NJ and parsimony (bootstrap support, BS). Asterisks (*) indicate a PP<95 or a BS<50. Prot, protostomians. To simplify the display, several nodes with a good support (PP>95 and BS⩾80) are marked by a filled circle; similarly the support for poorly supported nodes or for a few terminal nodes with average support was omitted. For the roots of the 'CavY extended' and 'Prot G1' groups the node support is indicated for two datasets, with the left-hand column derived from the complete dataset and the right-hand column derived from a reduced dataset where the two nematode sequences of the 'Prot G3' group were removed. For the root of the 'CavY extended' group the BS with the NJ analysis was <50 and the support with the Interior Branch Test is indicated in parentheses; the support on the left was for a 'CavY extended' group including the two nematode sequences of the 'Prot G3' group. The names of the species are colour-coded as indicated in the top-right corner of the figure.

occurred, and whether this can be timed relative to the emergence of *CavY*. Whereas the amphibian CavY has an ortholog in tunicates, two divergent sequences with no clear vertebrate orthologs are present in the genomes of *Ciona intestinalis* and *Ciona savignyi* (Cav-a and Cav-b) (Fig. 1). Interestingly their genes are localised on the same genomic segment and in the same transcription orientation (Fig. 2A), which is reminiscent of Cav1-Cav2 and Cav3-Cav2R in vertebrates. This is consistent with a model where the CavX-CavZ duplication took place before the split between vertebrates and urochordates, so that tunicates would possess an equivalent for both Cav1-Cav3, and Cav2-Cav2R (Fig. 2B). Although it is not possible to time the duplication that gave rise to CavY relative to that producing CavX and CavZ, CavY clearly arose before chordates split into urochordates and vertebrates (CavY minimum, Fig. 1) and probably before the split between protostomes and deuterostomes ('CavY extended', Fig. 1).

It is clear from the phylogenetic analysis that the ancestral caveolin gene has undergone ancient duplications. This plasticity of the caveolin family can be seen when the caveolin gene content is compared in detail within the different taxonomic groups. It then becomes evident that there were a large number of lineage-specific duplications and also gene loss. For example, in addition to the vertebrate-specific Cav1-Cav3, and Cav2-Cav2R duplications, several vertebrate species further expanded their caveolin gene content and, whereas humans only have three caveolins, bony fishes can have up to five caveolin genes (zebrafish Cav1, Cav2, Cav2R1, Cav2R2 and Cav3) and amphibians up to six (*X. tropicalis* Cav1, Cav2, Cav2R, Cav3-1, Cav3-2 and CavY). Such expansions are also seen in protostomes, particularly in molluscs, because *Lottia gigantean*, for example, possesses three to five genes that belong to the G1 group. Genetic loss is also extensive. With the exception of the amphibians, most vertebrates lack a CavY descendant, Cav2R was lost in placental mammals, the G1 group

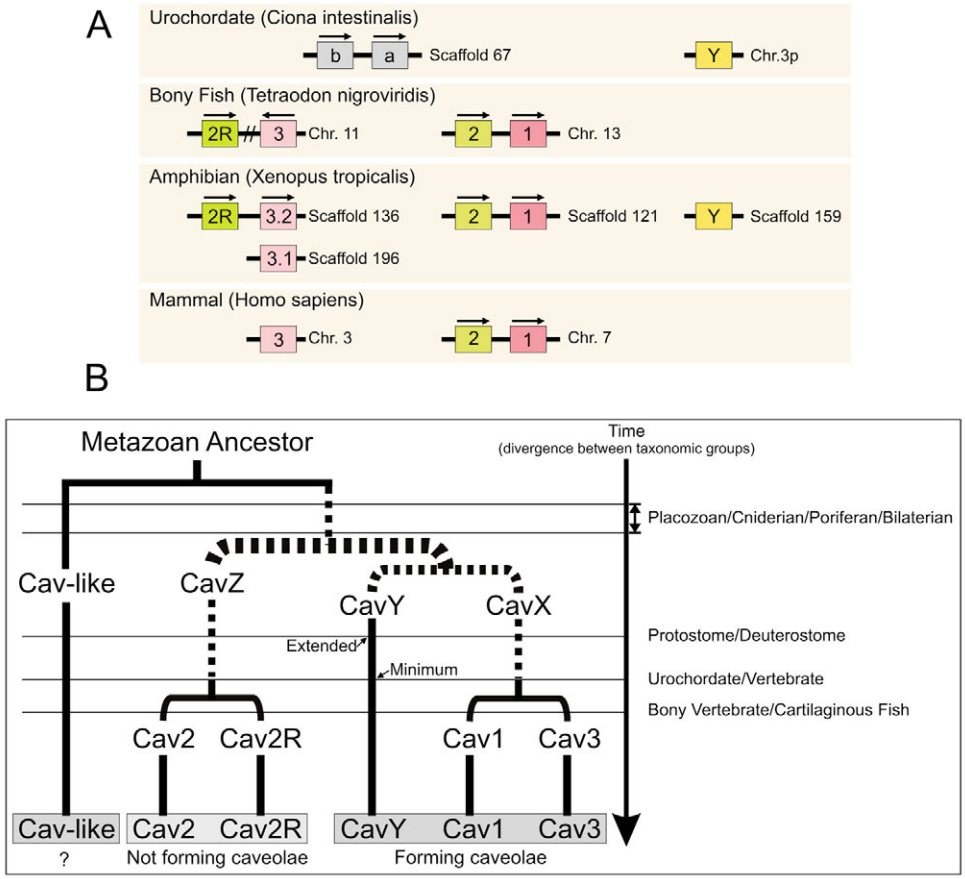

Fig. 2. Genomic organisation of caveolin genes and a model for the diversification of the caveolin sequences in metazoans. (A) Genomic localisation of caveolin-encoding genes in four species. Related families are indicated by related colours: Cav1 and Cav3 are pink, Cav2 and Cav2R are green and olive, respectively, and CavY-related sequences are yellow. When two genes are in a contiguous genomic segment the transcription orientation is indicated by an arrow above each gene. The symbol '//' between Cav2R and Cav3 in *Tetraodon nigroviridis* indicates a long genomic segment of ~1.3 Mb. (B) This model is based on the results of the phylogenetic analysis presented in Fig. 1 and summarises the interpretation in the text. For the parts of the model for which there is no clear phylogenetic support (represented by dotted lines), the simplest evolutionary model was selected based on the caveolin gene content information in the species studied and the ability of these sequences to form caveolae structures. For the CavY group, two levels of phylogenetic support are indicated: 'minimum' (supported by all the phylogenetic analysis methods used) and 'extended' (supported by two to three of the four methods used).

was lost in *D. melanogaster* (leaving flies without any caveolin) and many protostomes lack a G2 caveolin.

The high degree of conservation observed among caveolins from diverse species reveals the same general domain organization, allowing ready comparison of the roles of particular domains as well as sequence differences in caveola formation. To begin to address the question of when the ability to form caveolae arose during evolution, we examined whether caveola formation can be induced by caveolins from a number of different vertebrate and invertebrate species.

The transient expression of *Hs*Cav1 causes the de novo formation of caveolae in Cav1-null mouse embryonic fibroblasts (MEFs) from Cav1$^{-/-}$ mice (Kirkham et al., 2005). Microinjection of caveolin cDNAs, together with horseradish peroxidase (HRP) as a marker for the injected cells, allowed efficient electron microscopy (EM) analysis of caveola formation using a large number of different constructs. Cav1-null MEFs injected with cDNA encoding *Hs*Cav1 (Fig. 3B) or *Canis familiaris* Cav1-YFP (*Cf*Cav1-YFP) (not shown) showed similar distribution patterns of Cav1 labelling by light microscopy and formed surface-connected 65-nm vesicular or flask-shaped structures that were identical to those in wild-type MEFs as observed by EM (Fig. 3A). Similar results were obtained with *Hs*Cav1β (data not shown), *Mus musculus* Cav3-HA (*Mm*Cav3-HA) (Fig. 3C), *Danio rerio* Cav1-YFP (*Dr*Cav1-YFP) (data not shown) and, interestingly, even with the invertebrate *A. mellifera* Cav (*Am*Cav) (Fig. 3D). In stark contrast, nematode *Ce*Cav-a distribution was very uniform across the plasma membrane, without a clearly identifiable intracellular pool (Fig. 3E). Most importantly, *Ce*Cav-a did not induce the formation of recognisable caveolae as judged by EM (three independent experiments; data not shown).

To confirm and extend these studies, we developed a second EM experimental approach to test specific constructs for their ability to induce caveolae. This provided an opportunity to examine the efficiency and morphology of caveola production by different caveolin constructs at a range of expression levels and to also examine the effect of expression of flotillin-1 and flotillin-2, at similar expression levels. Cav1-null MEFs transiently transfected with GFP constructs were sorted by flow cytometry, based on fluorescence intensity, into pools of cells with high or low expression levels. These cells were then processed for EM analysis using Ruthenium Red to label the plasma membrane (Fig. 4). Clathrin-coated pits could be visualised in all samples processed and their density did not vary upon expression of the different constructs

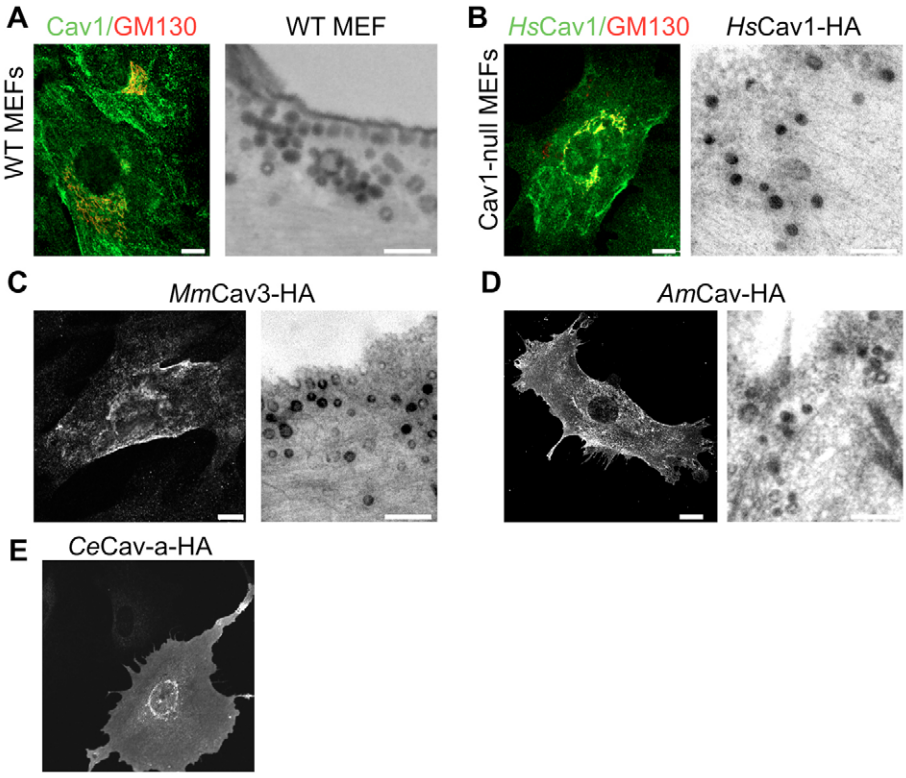

Fig. 3. Analysis of the de novo formation of caveolae in mammalian cells. (A) Wild-type MEFs were labelled with anti-Cav1 (green) and anti-GM130 (red) antibodies and prepared for confocal microscopy or surface-labelled with CTB-HRP and prepared for electron microscopy. (B-E) Using identical methodology, Cav1-null MEFs injected with HRP and either *Hs*Cav1-HA (B), *Mm*Cav3-HA(C) *Am*Cav-HA DNA (D) and *Ce*Cav-a-HA (E) and were prepared for both confocal and electron microscopy. All transiently expressed constructs, except *Ce*Cav-a-HA had the same subcellular distribution as Cav1 in wild-type MEFs as determined by confocal microscopy and produced surface-connected caveolae as identified with electron microscopy. Injected cells were identified by electron-dense HRP-DAB labelling of the nucleus. Scale bars: 10 μm (confocal images), 200 nm (EM images).

tested (data not shown). Caveolae and caveola-like structures were defined as 50-nm to 70-nm flask-shaped invaginations or smooth uncoated profiles positive for Ruthenium Red (i.e. surface connected). Ruthenium-Red-labeled profiles were quantified on random sections (Fig. 4F; see Materials and Methods). As expected, *Cf*Cav1 and *Hs*Cav1β both induced the formation of caveolae (Fig. 4A,C,F). However, in contrast to previous studies (Fujimoto et al., 2000), no difference was seen in the size, quantity or distribution of caveolae produced by the two constructs at either high or low expression levels in this experimental system (Fig. 4F). Furthermore, no significant induction of caveolae or caveola-like structures was observed in cells expressing *Ce*Cav-a (Fig. 4D,F) or coexpressing flotillin-1 and flotillin-2 (Fig. 4A,F) as compared with control cells that express only GFP (Fig. 4B,F). In parallel, the coexpression of flotillin-1-GFP and flotillin-2-RFP in transfected cells was confirmed by light microscopy. Interestingly, the transient coexpression of flotillin-1 and flotillin-2 caused a small but significant increase in tubular membrane structures (see supplementary material Fig. S2) morphologically similar to those implicated in a non-clathrin non-caveolae endocytic pathway (Kirkham et al., 2005). These structures were morphologically distinct from caveolae.

Taken together, these results show that in a heterologous expression system, caveolin from a wide range of species – including invertebrates – can induce caveola formation; however, this is not a universal feature of all caveolins. We found that caveolae produced during the transient expression of mammalian Cav1, Cav1β and Cav3, vertebrate *Dr*Cav1 and invertebrate *Am*Cav all had the same morphology. Remarkably, insect *Am*Cav could form caveolae in a mammalian cell despite differences in membrane temperature, lipid and/or sterol composition (Marheineke et al., 1998), and lipid and/or sterol structure (Rietveld et al., 1999). This highlights the evolutionary conservation of caveola formation, even in cells with distinct lipid composition (Rietveld et al., 1999). Furthermore, because caveolae-forming caveolins are found in CavX and possible CavY descendants, we predict that the ancestral caveolin was able to form caveolae.

If functionality is taken into account in terms of understanding CavX-CavZ duplication, a parsimonious scenario would extend the timing of a CavX-CavZ duplication to before the split between the protostomes and deuterostomes (Fig. 2). Then, CavZ would have given rise to *Ce*Cav-a (protostomian G2 group) and the vertebrate Cav2-Cav2R clade, none of which form caveolae. But given the ambiguity in timing the appearance of CavZ, it is also possible that *Ce*Cav-a and mammalian Cav2 experienced a convergent loss of function.

These results prompted us to analyse whether *Ce*Cav-a and *Hs*Cav1 differed in other properties. First, we used total internal reflection fluorescence microscopy (TIRF) to further examine the distribution of *Ce*Cav-a at the plasma membrane of Cav1-null MEFs. Cav1-null MEFs that express *Hs*Cav1-HA clearly exhibited punctate fluorescent structures (supplementary material Fig. S3). By contrast, *Ce*Cav-a-HA showed a uniform distribution at the plasma membrane, consistent with the inability of *Ce*Cav-a to induce caveola formation (supplementary material Fig. S3). Second, *Hs*Cav1 showed a polarised distribution in migrating fibroblasts, consistent with previous work (Sun et al., 2007) but *Ce*Cav-a showed a non-polarised uniform distribution over the cell surface (supplementary material Fig. S4). Third, *Hs*Cav1 inhibited the uptake of the cholera toxin B subunit when expressed in Cav1-null MEFs, consistent with previous studies (Kirkham et al., 2005), but *Ce*Cav-a had no detectable inhibitory effect (supplementary material Fig. S3). Fourth, *Hs*Cav1, but not *Ce*Cav-a, redistributed to lipid droplets upon treatment of cells with fatty acids (supplementary material Fig. S4). Finally, in cells transfected with the constitutively active form of Rab5 ($Rab5^{Q79L}$), *Ce*Cav-a, but not *Hs*Cav1, accumulated in $Rab5^{Q79L}$-enlarged endosomes (supplementary material Fig. S4). This is consistent with infrequent budding of caveolae in unstimulated cells (Kirkham et al., 2005; Thomsen et al., 2002), and endocytosis of the non-caveolar *Ce*Cav-a via clathrin-coated pits (Sato et al., 2006). Whether the functional pool of *Hs*Cav1 in

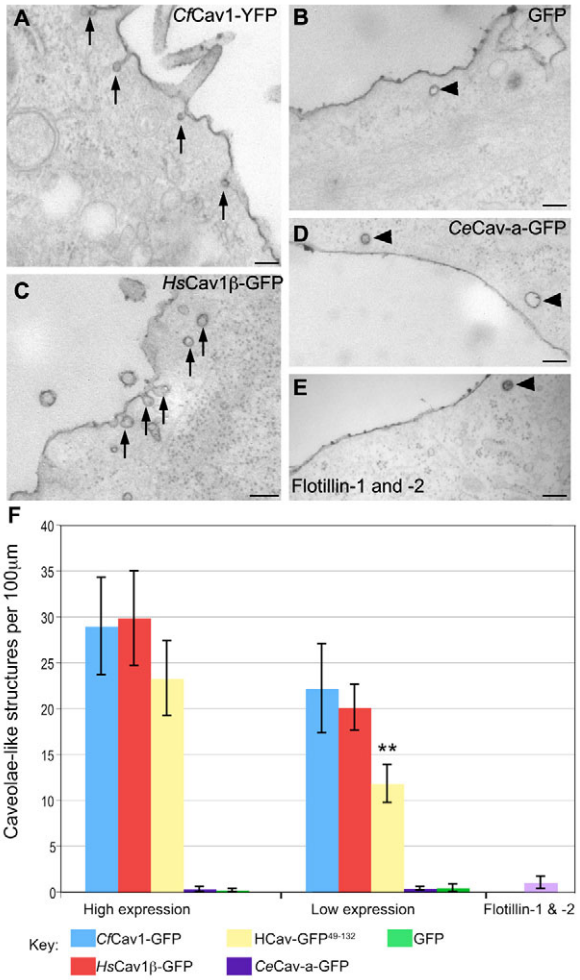

Fig. 4. Quantification of the de novo formation of caveolae in mammalian cells. (A-F) Cav1-null MEFs transiently transfected with *Cf*Cav1-YFP (A,F), GFP (B,F), *Hs*Cav1β-GFP (C,F) *Ce*Cav-a-GFP (D,F), HCav$^{49\text{-}132}$-GFP (F) or co-transfected with flotillin1-GFP and flotillin2-RFP (E,F), were FAC sorted by fluorescent intensity into two pools with different expression levels with the exception of flotillin-1 and flotillin-2. The cells were fixed and examined by electron microscopy. Caveolae (arrows) were only observed in cells transfected with *Cf*Cav1-GFP, *Hs*Cav1β-GFP and at a lower frequency in cells expressing HCav$^{49\text{-}132}$-GFP. Clathrin-coated pits are highlighted by arrowheads. Scale bars: 200 nm. (F) Caveolae-like structures as determined by morphology were counted at the plasma membrane and the density of caveolae-like structures was determined. $^{**}P \leqslant 0.05$, difference between high and low expression pools of the same construct.

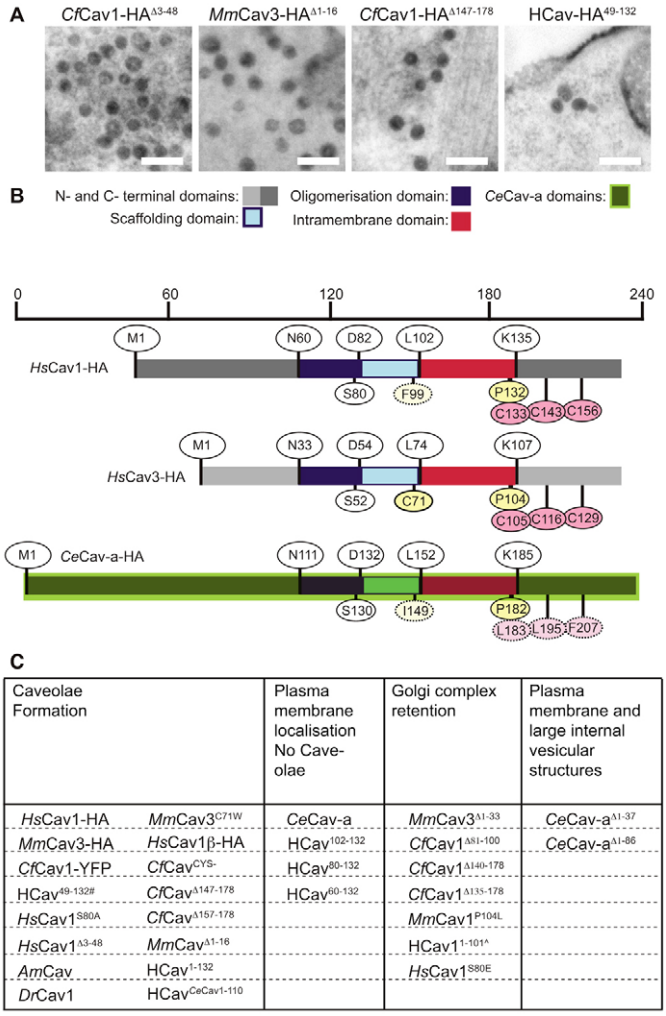

C

Caveolae Formation		Plasma membrane localisation No Cave-olae	Golgi complex retention	Plasma membrane and large internal vesicular structures
*Hs*Cav1-HA	*Mm*Cav3^{C71W}	*Ce*Cav-a	*Mm*Cav3$^{\Delta 1\text{-}33}$	*Ce*Cav-a$^{\Delta 1\text{-}37}$
*Mm*Cav3-HA	*Hs*Cav1β-HA	HCav$^{102\text{-}132}$	*Cf*Cav1$^{\Delta 81\text{-}100}$	*Ce*Cav-a$^{\Delta 1\text{-}86}$
*Cf*Cav1-YFP	*Cf*Cav^{CYS-}	HCav$^{80\text{-}132}$	*Cf*Cav1$^{\Delta 140\text{-}178}$	
HCav$^{49\text{-}132\#}$	*Cf*Cav$^{\Delta 147\text{-}178}$	HCav$^{60\text{-}132}$	*Cf*Cav1$^{\Delta 135\text{-}178}$	
*Hs*Cav1^{S80A}	*Cf*Cav$^{\Delta 157\text{-}178}$		*Mm*Cav1^{P104L}	
*Hs*Cav1$^{\Delta 3\text{-}48}$	*Mm*Cav$^{\Delta 1\text{-}16}$		HCav1$^{1\text{-}101\wedge}$	
*Am*Cav	HCav$^{1\text{-}132}$		*Hs*Cav1^{S80E}	
*Dr*Cav1	HCav$^{CeCav1\text{-}110}$			

Fig. 5. Summary of the 33 different caveolin constructs analysed. (A) EM micrographs of Cav1-null MEFs microinjected with HRP and either *Hs*Cav-HA$^{\Delta 3\text{-}48}$, *Mm*Cav3-HA$^{\Delta 1\text{-}16}$, *Cf*Cav1-HA$^{\Delta 147\text{-}178}$ or HCav-HA$^{49\text{-}132}$ DNA. The cell surface was labelled with CTB-HRP. All the constructs generated caveolae that were similar to endogenous caveolae in wild-type MEFs. Scale bars: 200 nm. (B) Schematic protein alignment illustrating the protein-domain structure and some of the known post translational modifications of *Hs*Cav1, *Hs*Cav3 and *Ce*Cav-a. The scale bar indicates the number of amino acids from the start of the N-terminus of *Ce*Cav-a. Pink circles highlight palmitoylated residues, yellow circles mark some of the residues mutated in *Hs*Cav3 in muscle diseases. Circles with broken lines and lightly shaded mark non-conserved residues. (C) Summary of the results of EM and light-microscopy experiments from the constructs tested in this study. #, constructs that formed caveolae but were less efficient than wild-type constructs. ^ , 20% of cells expressing this construct contained more peripheral structures, but these were judged not to be caveolae by light microscopic methods.

all these assays is within caveolae is not clear but, taken together, these results suggest that, caveolins that do not drive caveolae formation have distinct properties and, presumably, at least some distinct functions.

Molecular dissection of caveola formation

To gain insights into formation of caveolae, we examined the importance of posttranslational modifications of caveolins or the effect of previously described mutants of caveolins – many of which have been associated with disease – on caveola formation in Cav1-null MEFs using the assays described above (see Fig. 3). The results are summarised in Figs 5 and 6. A triple point mutant of *Cf*Cav (*Cf*Cav1-HA^{CYS-}) that cannot be palmitoylated, was localised to the plasma membrane using confocal microscopy and formed caveolae identical to those found in wild-type MEFs – as judged by EM (supplementary material Fig. S5). Mammalian Cav1 is phosphorylated at Y14 and S80. The Y14 residue can be deleted without affecting caveolae formation because both *Hs*Cav1β (Fig. 4) and *Cf*Cav1$^{\Delta 3\text{-}48}$ (Fig. 5A) can generate caveolae; although, if Y14 is present it may have a regulatory role on caveola formation (Orlichenko et al., 2006). We also analysed Cav1-null MEFs that express the non-phosphorylatable point mutant *Hs*Cav1^{S80A}. The *Hs*Cav1^{S80A} mutant protein was localised to the plasma membrane

and capable of forming caveolae, as determined by the EM caveola-biogenesis assay (supplementary material Fig. S5). By contrast, *Hs*Cav1^{S80E}, which mimics chronic phosphorylation of this residue, was localised almost exclusively to the Golgi complex (supplementary material Fig. S5). Therefore, phosphorylation of *Hs*Cav1^{S80} is not required for caveola formation, but it may regulate caveolin and/or caveolae trafficking to or from the plasma membrane. Other mutants of Cav3 implicated in muscular dystrophy were either retained in the Golgi complex (*Mm*Cav3^{P104L}) or generated apparently normal caveolae (*Mm*Cav3^{C71W}) (data summarised in Fig. 5).

Analysis of the C-terminus and the intramembrane domain of caveolins in the formation of caveola

To gain more insights into the requirements for caveola formation, we took advantage of the fact that *Ce*Cav-a efficiently traffics to the plasma membrane and used *Ce*Cav-a as a backbone to introduce mammalian caveolin domains that may facilitate the formation of caveola. We first focused on the C-terminal half of caveolin, where the last 31 amino acids can be deleted without affecting caveolae formation (summarised in Figs 5, 6, and supplementary material Fig. S5). In addition, *Cf*Cav1$^{\Delta147\text{-}178}$ showed reduced plasma membrane localisation as compared with *Hs*Cav1-HA and *Cf*Cav1$^{\Delta157\text{-}178}$. Notably, a progressive reduction in caveolin oligomerisation, and plasma membrane localisation that was proportional to the severity of the deletion, has been reported earlier (Ren et al., 2004).

Next, we analysed the hybrid protein HCav-HA$^{1\text{-}132}$, where the amino acid residues 1-132 of the hybrid protein originate from residues 1-132 of *Hs*Cav1 and the remaining C-terminal amino acids are from *Ce*Cav-a (schematic of Hybrid: Fig. 6). All hybrid mutants are named after the segment originating from *Hs*Cav1. HCav-HA$^{1\text{-}132}$ formed caveolae that were morphologically similar to *Hs*Cav1 (data not shown), clearly indicating that the C-termini of *Hs*Cav1 and *Ce*Cav-a, in particular amino acids 132 to 147, are functionally equivalent. The C-terminus of mammalian Cav2 has been previously shown to support caveola biogenesis when present in a hybrid protein with mammalian Cav1 (Breuza et al., 2002). Closer inspection of all mammalian Cav1, Cav2, Cav3 and *Ce*Cav-a C-termini (Fig. 6, supplementary material Fig. S1) highlights several conserved amino acid residues, such as P132 and K135. Furthermore, mammalian Cav1, Cav2 and Cav3 contain a series of four hydrophobic residues in an n+3 spacing, which comprises leucines, isoleucines and valines that are partly conserved in *Ce*Cav-a (Fig. 6). The importance of this region has further been highlighted by the fact that four out of six newly identified mutations in human breast cancer are located between amino acid residues P132 and Y148 in *Hs*Cav1 (Fig. 6) (Li et al., 2006).

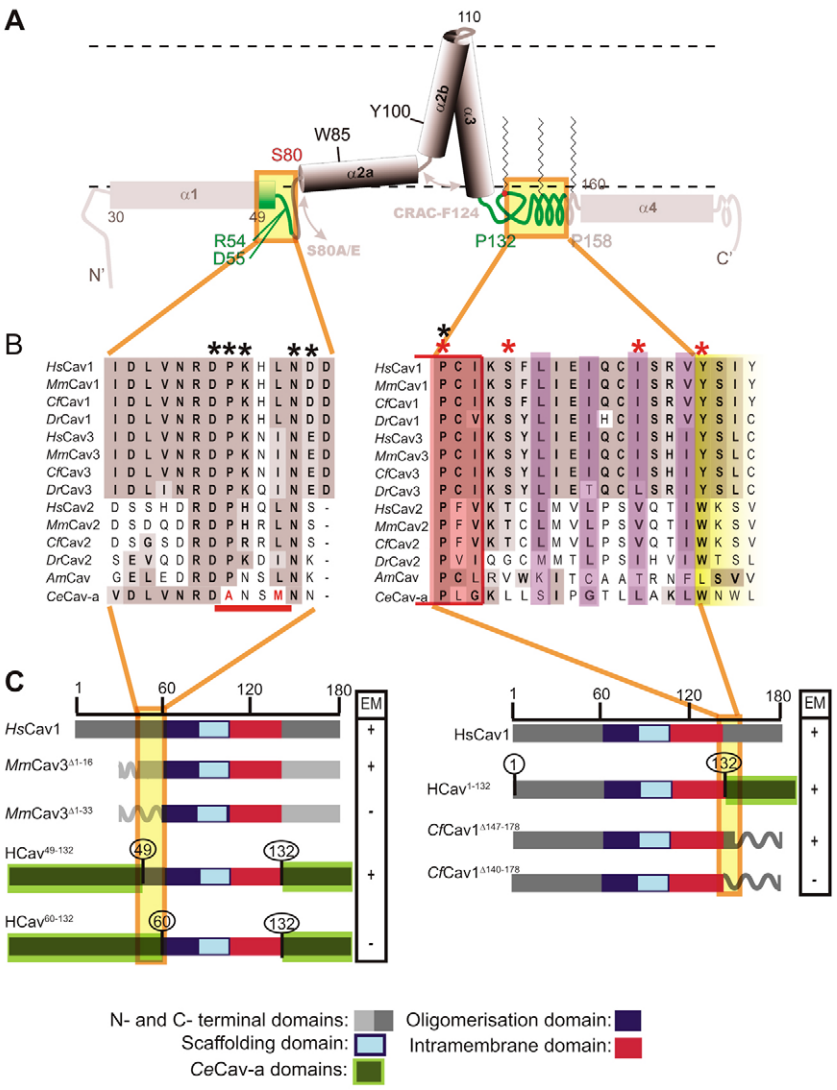

Fig. 6. Analysis of caveola formation using deletion mutants and hybrid proteins. (A) Topology model of caveolin. Orange boxes mark the region of interest that are shown in alignments below. (B) Sequence alignment. Dark grey, identical residues; light grey, similar residues; purple, partly conserved hydrophobic residues; red asterisks, residues mutated in breast cancer; shaded yellow region, residues that can be deleted without affecting caveola formation; red line and red text, residues that are not conserved in *Ce*Cav-a compared with all other sequences in the alignment; black asterisks, residues implicated in muscular dystrophy when mutated in *Hs*Cav3. (C) Caveolin mutants used in this study. Grey, N- and C-terminal regions; dark blue, oligomerisation domain; light blue, scaffolding domain; red, intramembrane domain. Curved lines indicate missing sections. Regions highlighted in green are from *Ce*Cav-a. Orange, regions of interest that are shown in alignments. + and – presence and absence, respectively, of caveolae according to the results of the EM caveola biogenesis assay. Scale bars indicate the number of amino acids.

Finally, we created the hybrid protein HCav$^{1\text{-}102}$ that containes only the N-terminal region from *Hs*Cav1(1-102). This construct did not induce caveola formation, as demonstrated through a range of EM and light-microscopy assays, but did reach the plasma membrane in a small subset of cells (supplementary material Figs S5, S6). Hence, the intramembrane domain of *Ce*Cav1 cannot substitute for the intramembrane domain of *Hs*Cav1, while the C-termini have equivalent function.

It is interesting to note that the intramembrane domains of *Ce*Cav-a and mammalian Cav1 are highly conserved, comprising mostly conservative amino acid substitutions (supplementary material Fig.

S1) – with three notable exceptions. These involve residues S104, F124 and A129, which in *Ce*Cav-a are replaced by a valine, serine and isoleucine, respectively. Each residue is completely conserved in vertebrate Cav1 (supplementary material Fig. S1), and each of these changes causes a dramatic change in side-chain hydrophobicity (S/V, 0.46 to –0.46; F/S, –1.71 to 0.46; A/I, 0.50 to –1.12) as determined by Wimley and White (Wimley and White, 1996). Intriguingly, a microdeletion of F124 is known to cause muscular dystrophy (Cagliani et al., 2003) and, of those residues, F124 is the only one conserved in *Am*Cav but not *Ce*Cav-a (supplementary material Fig. S1).

Role of the N-terminus of caveolin in caveola formation

To analyse a potential role of the N-terminus in caveola formation, we examined a series of N-terminal truncation mutants of mammalian Cav1 and Cav3. The first 48 amino acids of *Cf*Cav1 or the equivalent region of *Mm*Cav3 can be deleted without affecting its ability to form caveolae (summarised in Figs 5, 6).

Next, we created further hybrid proteins between *Hs*Cav1 and *Ce*Cav-a with increasing proportions of the N-terminal region of *Ce*Cav-a replacing corresponding regions of *Hs*Cav1. *Ce*Cav-a possesses a unique N-terminal extension that is missing in mammalian isoforms. First, we determined through a series of deletion mutants and hybrid proteins that this N-terminal extension did not inhibit caveolae formation (supplementary material Fig. S5). Of all the hybrid proteins designed specifically to analyse the N-terminal region (summarised in Figs 5, 6), only HCav$^{49\text{-}132}$ (*Hs*Cav1 amino acid residues 49-132) was capable of forming caveolae (Figs 4-6). Examination of transfected cells using confocal microscopy showed some regions of the plasma membrane with a diffuse surface distribution of HCav$^{49\text{-}132}$ (supplementary material Fig. S5). To investigate this further, we quantified the caveolae produced by HCav$^{49\text{-}132}$ by using the quantitative EM assay described in Fig. 4. HCav$^{49\text{-}132}$ did not produce caveolae with an abnormal morphology but produced caveolae less efficiently. At the lower expression level HCav$^{49\text{-}132}$ was far less efficient than wild-type caveolin in generating caveolae. Importantly, HCav$^{60\text{-}132}$ that contained only 11 more amino acids from *Ce*Cav-a, failed to form caveolae as determined by both the EM biogenesis assay (data not shown) and TIRF microscopy (supplementary material Fig. S6). These results confirm the importance of amino acids 48-60 in caveola formation. The region 46-55 has recently been implicated in localising caveolin correctly in migrating fibroblasts (Sun et al., 2007).

Based on our sequence alignments this region can be confined further. As residues 50-55 of *Hs*Cav1 are identical between vertebrate Cav1 and *Ce*Cav-a, the first crucial amino acid for *Hs*Cav1 is likely to reside between residues 56 and 59 (supplementary material Fig. S1). This region contains the residue equivalent to the Cav3 muscular dystrophy mutant Cav3^{P28A} (Betz et al., 2001). Intriguingly, this phenylalanine is conserved in *Am*Cav but substituted by an alanine residue in *Ce*Cav-a (marked in red in Fig. 6B). Other signature residues that distinguish the caveola-forming sequences from those that do not form caveolae include G77, C133 and S149. Although C133 and S149 are either outside the regions required for caveola formation or can be mutated without inhibiting formation of caveola, these residues might still facilitate efficient caveola formation in vivo.

Finally, we asked whether caveola formation is dependent on the interaction of the hybrid Cav proteins with Cav2. In Cav1-null MEFs endogenous *Mm*Cav2 is localised to the Golgi complex but redistributes to the plasma membrane upon transient overexpression of *Hs*Cav1 (supplementary material Fig. S6) (Mora et al., 1999). We therefore analysed our HCav hybrid mutants for the loss of Golgi-complex-localised *Mm*Cav2. Surprisingly, all hybrid proteins were capable of interacting with *Mm*Cav2, independently of their ability to form caveolae (supplementary material Fig. S5). Thus the specific interaction with Cav2 is not an indicator of caveola formation.

Discussion

In this study we have carried out a detailed phylogenetic analysis of caveolins. In addition, we analysed the ability of caveolins from different species, as well as mutant forms of caveolin, to cause the de novo formation of caveolae in mammalian cells. We have shown that, although caveolins are conserved in evolution, their ability to cause formation of caveolae in this model system is not. Whereas many mutants of mammalian caveolins accumulate in the Golgi complex, we have shown that *C. elegans* caveolin reaches the plasma membrane but does not form caveolae. This finding allowed us to generate hybrid proteins by using *C. elegans* caveolin as a scaffold and to generate a new model of caveola formation. Surprisingly, we found that coexpression of flotillin-1 and flotillin-2 did not cause the formation of caveola-like structures in our experimental system. Previous studies showed an increase in caveola-like invaginations on expression of flotillin-1 and flotillin-2 (Frick et al., 2007). In contrast to those studies, the experiments described here were performed in cells that lack caveolae and Cav1. We conclude that within cells that lack Cav1 either flotillin-1 and flotillin-2 cannot induce caveola-like structures, or these structures are very dynamic once formed and are quickly endocytosed. It is interesting to note that the coexpression of flotillin-1 and flotillin-2 caused an increase in tubular structures (supplementary material Fig. S2) with similar morphology to clathrin-independent endocytic carriers (CLICs) (Kirkham et al., 2005). This pathway is regulated by flotillin-1 (Glebov et al., 2006) but further work will be required to dissect the precise role of flotillin-1 in CLIC formation and/or dynamics.

A systematic phylogenetic analysis of caveolin sequences indicates that caveolins in vertebrates originate from three ancestral genes: *CavX*, *CavZ* and *CavY* (Fig. 2B). Using a mammalian-cell-based assay to study the de novo formation of caveolae, we found that both descendants of CavX (mammalian Cav1 and Cav3, vertebrate *Dr*Cav1) and CavY descendants (invertebrate *Am*Cav) formed morphologically similar caveolae. This highlights the evolutionary conservation of caveola formation and indicates that the CavY-CavX ancestral caveolin was able to form caveolae. However, there is not uniform conservation of caveolin formation in the animal lineage. In contrast to the caveola-forming *Am*Cav from *A. mellifera*, another invertebrate caveolin – *Ce*Cav-a from *C. elegans* – does not form caveolae.

We then extended the study to gain insights into how caveolin forms caveolae. The analysis of chimeric caveolins and mutants based on sequence comparison of caveolins with differential ability to form caveolae revealed that residues 49-147 in mammalian Cav1 are required for caveola formation. No wild-type caveolin construct (from mammals to invertebrates) and no mutant caveolin formed caveolae of abnormal morphology, as judged by conventional EM. Rather than producing abnormal caveolae, a reduction in the efficiency of caveola formation was observed. Thus, caveola formation seems to be a binary event, i.e. all or nothing. This included caveolae produced by expression of *Mm*Cav3^{C71W}, equivalent to a possible polymorphism originally implicated in muscular dystrophy (de Paula et al., 2001; McNally et al., 1998;

Vatta et al., 2006), which – when expressed in fibroblasts – inhibits specific cholesterol-dependent signalling pathways (Carozzi et al., 2002).

We provide evidence that caveolin genes underwent extensive and ancient local and genomic gene duplication to produce diversity in caveolin function. We have analysed information on the genomic organisation of caveolin genes and combined this with the phylogenetic analysis to suggest a model for the ancient evolution of the three main groupings of caveolins: CavX, CavY and CavZ (Fig. 2B). The precise timing of the two duplications that gave rise to these three groupings is unclear, although at least one duplication took place before the split between vertebrates and urochordates, and both possibly occurred even before the split between protostomes and deuterostomes (Fig. 2B). There is also evidence for other genomic gene duplication and loss in the caveolin gene family. It would seem that, during vertebrate speciation, a genetic segment containing ancestral *CavX* and *CavY* duplicated to give rise to *Cav1* and *Cav2*, and *Cav3* and *Cav2R* with subsequent loss of *Cav2R* in placental mammals. Also, in most vertebrates except amphibians, it appears the *CavY* descendant was lost. Furthermore, there are numerous duplicates of caveolin genes in non-vertebrate species that are more closely related to each other than to caveolins of other species (Fig. 1).

This caveolin gene plasticity is in dramatic contrast to the very limited diversification of clathrin heavy and light chain genes, which also encode proteins involved in membrane-coat formation. The genes for clathrin subunits are present in all eukaryotic lineages, whereas caveolins are limited to metazoans (Field et al., 2007). In the animal kingdom there is only one gene that encodes clathrin heavy chain and one that encodes clathrin light chain in non-vertebrate species, and there is evidence for only limited duplication in the vertebrate lineage (Wakeham et al., 2005). The more recent emergence and greater variability of caveolin genes may reflect considerably more flexibility in function for caveolins than for clathrin. Although caveolins and their ability to form caveolae are evolutionarily conserved, it appears that there has been also a conserved divergence of function in the caveolin family. In *C. elegans*, and in the Cav2-Cav2R lineage of vertebrates, the ability of caveolin to form caveolae is lost. Genes encoding caveolins that do not form caveolae arose from an ancient duplication in the metazoan lineage (Fig. 2). The fact that they survived selection and have been retained, strongly suggests they have a function.

*Ce*Cav-a behaved differently to mammalian caveolin in a wide range of cellular processes including the redistribution to de-novo-formed lipid droplets, the relocation to the rear of migrating fibroblasts, and the failure to cause an inhibition of clathrin-independent endocytosis. In addition, *Ce*Cav-a but not *Hs*Cav1 accumulated within enlarged early endosomes when expressed with a dominant-active Rab5 mutant. This observation suggested that incorporation of caveolins into caveolae results in their retention at the surface, preventing internalisation, or allows their rapid recycling so that those caveolins that do not form caveolae have a less-restricted localization in the endocytic pathway. Internalisation of non-caveolar *Ce*Cav-a is consistent with in vivo studies in the *C. elegans* embryo where *Ce*Cav-a has been demonstrated to be internalised via a clathrin-dependent process (Sato et al., 2006). Intriguingly, a recent report has indicated that *Ce*Cav-a has some functional similarities to mammalian caveolins at the neural muscle junction (Parker et al., 2007). Whether this involves caveolae is not yet known but it is important to note that, even in mammalian cells, there is increasing evidence for non-caveolar functions of caveolins (Head et al., 2007; Hill et al., 2008; Parton and Simons, 2007).

The role of caveolin in caveola formation – a model

By combining the increased understanding of caveolin evolution with the molecular analysis of an array of caveolin constructs we were able to refine a model of caveolae formation. On the basis of a variety of secondary structure and hydrophobicity prediction algorithms, we previously presented a topology model for *Mm*Cav1 (Parton et al., 2006), which can now be significantly refined (Fig. 6). The model predicted caveolin-caused membrane curvature through the insertion into one membrane leaflet of an amphipathic α-helices (*Mm*Cav1 resides 80-95) and the interaction of cholesterol with the intramembrane domain of caveolin, such that the helix acts like a wedge, displacing lipids in the inner but not the outer membrane leaflet, and thus create membrane curvature (McMahon and Gallop, 2005). At the time it was possible that the extreme N- and C-termini were necessary to stabilise the overall protein conformation. Regarding the complete dispensability for caveola formation of segments 1-49 and 157-178 in *Hs*Cav1, we can now rule out such a requirement. An alternative, based on the requirement of segment 49-60 for caveola formation, could be that this segment has a stabilizing function for the in-plane α-helix (Parton et al., 2006; Spisni et al., 2005) (Fig. 6). It is likely to be influenced by phosphorylation of S80, which should result in a relocation of this helix into the membrane interface region. Such a scenario is supported by the fact that *Hs*Cav1^{S80A} has an increased affinity for cholesterol (Fielding et al., 2004) and our observation that *Hs*Cav1^{S80A} but not *Hs*Cav1^{S80E} is capable of caveola formation (Fig. 4). These findings highlight a potential regulatory role of this highly conserved residue in caveolae formation and function and possibly also caveolae disassembly.

Additional elements that may help to stabilise caveolin in caveolae might also be present in the C-terminus. The segment 132-147 contains a series of four hydrophobic residues in an n+3 spacing comprising leucines, isoleucines, and valines (Fig. 6B) that may insert into the membrane or alternatively, be involved in caveolin oligomerisation. The slight loss in plasma membrane localisation of *Cf*Cav1$^{147-178}$ but not *Cf*Cav1$^{157-178}$ might be the result of cutting into this structure. It has been reported that the severity of the deletion of the C-terminus is proportional to the reduction in caveolin oligomerisation and plasma membrane localization (Ren et al., 2004). Thus the increasing removal of functional residues that could help to stabilise the C-terminal region might lead to a progressive reduction in the efficiency of caveolae production, although the loss of any one such element, e.g. palmitoylation, is dispensable.

With respect to the intramembrane domain, our model places residue F124 within the intramembrane domain at the same penetration depth as the segment 97-YWFY-100, which forms part of the CRAC motif and is believed to be involved in cholesterol binding (Li and Papadopoulos, 1998; Parton et al., 2006). F124 was conserved in caveola-forming caveolin and interaction of these residues might be necessary for a stable interaction between inward and outward helices of the intramembrane domain. Bulky residues between these two helices close to the membrane interface, combined with a tight turn of residues 108-GIPM-111 in the hydrocarbon core, might result in a cone-shaped intramembrane domain. Although we previously assumed that the intramembrane domain increases the volume of both membrane leaflets equally

(Parton et al., 2006), this might contribute further to the creation of membrane curvature.

We propose that caveolin causes membrane deformation of the cytoplasmic leaflet through a combination of amphipathic helix insertion and interaction with cholesterol. The membrane deformation is then stabilised and concentrated through oligomerisation of caveolin and the interaction with cholesterol. These steps, fundamental for caveola formation, are mediated by different regions of caveolin. This would explain the wide range of caveolin mutations that affect caveola formation. This model does not preclude the involvement of other proteins or lipids in regulating caveola formation. In fact, recent studies suggest that other proteins can regulate caveolae stability or formation driven by caveolin (Hill et al., 2008; Pelkmans and Zerial, 2005). These studies provide a framework for understanding the mechanics of membrane morphogenesis by caveolins, the regulation of this process in vivo, and provide fundamental new insights into the evolution of caveolae and caveolins.

Materials and Methods

Cell culture and cell treatments

BHK cells were grown in DME (Invitrogen, Carlsbad, CA) supplemented with 10% (v/v) heat-inactivated Serum Supreme (Cambrex Bio Science, Australia) and 2 mM L-glutamine (Invitrogen). Primary cultures of MEFs were isolated and cultured as described previously (Kirkham et al., 2005). Lipid-based transfection of cells were performed using Lipofectamine 2000 (Invitrogen) according to manufacturer's instructions. Oleic acid treatment was performed as previously described (Pol et al., 2004). The uptake and measurement of CTB conjugated to Alexa Fluor 594 (Invitrogen) within the Golgi complex was performed as described previously (Kirkham et al., 2005).

Antibodies and reagents

Antibodies were obtained from the following sources: rabbit anti-caveolin, mouse anti-GM130 and mouse anti-Cav2 (BD Biosciences, San Jose CA), rabbit anti-HA (provided by T. Nilsson, Gothenburg University, Sweden), mouse anti-HA (16B12) (BabCO, Richmond, CA), mouse anti-Flag and rabbit anti-Flag (Sigma-Aldrich). Secondary antibodies conjugated to Alexa Fluor 488 and 660 (Invitrogen) and to CY3 (Jackson ImmunoResearch Laboratories, West Grove, PA). An extensive summary of the DNA constructs used in this study is contained in a Table S2 in supplementary material. Constructs created for this study were generated by primer-extension PCR (primer sequences can be given by request) or are described in previous studies (Carozzi et al., 2002; Fielding et al., 2004; Luetterforst et al., 1999; Ren et al., 2004; Scheel et al., 1999; Stenmark et al., 1994; Way and Parton, 1996). All new constructs generated were sequenced (AGRF, Brisbane, Australia).

EM caveola biogenesis assay

Primary cell cultures of Cav1-null and wild-type MEFs were microinjected as previously described (Kirkham et al., 2005) with 10 mg/ml HRP in the injection mix. All the cells in a defined area, roughly five to ten cells across and 15-30 cells down, were microinjected and allowed to recover in normal growth medium for 12-15 hours at 37°C in 5% CO_2. The plasma membrane of injected cells was labelled on ice with 10 μg/ml CTB-HRP (Invitrogen) as previous described (Kirkham et al., 2005). The cells were processed for DAB visualisation and resin embedding using standard protocols (Kirkham et al., 2005) with the following modification. Injected cells with DAB reaction product in the nucleus were relocated after embedding by making marks in the plastic dish after the DAB reaction. The marked area was then identified and the cells were cut parallel to the culture substratum. In parallel cells grown on a glass coverslip were injected using the same injection mix and the protein expression level was determined by immunofluorescent confocal analysis.

Cells with HRP-positive nuclei were analysed by electron microscopy for CTB-HRP-positive structures and were compared with neighbouring non-injected cells. A negative results were adjudged by no noticeable different between injected and non-injected cells in the morphology and distribution of CTB-HRP positive structure. Positive results were adjudged by the appearance of 50-nm to 70-nm flask-shaped invaginations or smooth uncoated vesicles in different planes.

Flow cytometry and EM analysis

Cav1$^{-/-}$ immortalised MEFs were transfected using Lipofectamine LTX was used with PLUS reagent (Invitrogen) overnight with various GFP-tagged caveolin constructs, or co-transfected with flotillin-1-GFP and flotillin-2-RFP at a ratio of 1:3, so that all cells expressing flotillin-1-GFP expressed flotillin-2-RFP (as tested in parallel using light microscopy). Cells were trypsinised the next day, and the cell suspension was sorted by GFP fluorescence using a Influx Cell Sorter (Cytopeia). The GFP-positive population was sorted into two wells of a 24-well plate based on the intensity of GFP. Roughly 10% of cells were sorted into high-GFP or low-GFP wells for all the caveolin constructs, giving a ~20% transfection rate. Note that only low-GFP expressors were obtained for flotillin-1 and flotillin-2. Cells were sorted into growth medium containing penicillin-streptomycin, and placed in 5% CO_2 incubator for 4 hours. Unattached cells were washed off, and fresh medium with penicillin-streptomycin was added for a further 3-hour incubation prior to fixation in 2.5% glutaldehyde containing 1 mg/ml Ruthenium Red for 1 hour at RT.

Labelling of the cell surface by Ruthenium Red and Epon resin embedding was performed as previously described (Parton et al., 2002). Quantification of surface-connected structures was performed on over 500 μm of plasma-membrane profile for each condition. A 1000-nm square grid was superimposed over the electron micrograph and the cell perimeter calculated based on the number of intersections with the grid lattice. All Ruthenium Red-positive structures were tallied per cell. Total number of caveolae or caveolae-like structures were divided by the calculated cell perimeter and multiplied by 100 to give caveolae per 100 μm plasma-membrane profile.

Immunofluorescence microscopy

Cells were fixed and prepared for immunofluorescence microscopy as previously described (Kirkham et al., 2005) with only minor modifications. Cells visualised by TIRF microscopy were mounted in PBS-containing 0.5% n-propyl gallate, all other samples were mounted in Aqua-polymount (Polysciences Inc., Warrington, PA). Lipid droplets were visualised as previously described (Martin et al., 2005). Confocal immunofluorescence microscopy was performed using a Zeiss LSM 510 meta confocal microscope. Images were processed using Zeiss confocal microscopy software version 3.2 and Adobe Photoshop version 7, and figures were compiled using Adobe Illustrator version 10 and Microsoft Powerpoint X. TIRF microscopy was performed using an Olympus X81 inverted microscopy adapted for TIRF microscopy (by Olympus), Images were processed and analysed using Metamorph software.

Dataset and phylogenetic analysis

To constitute the caveolin dataset an initial BLAST (Altschul et al., 1990) search was performed to screen NCBI's non-redundant database and all the caveolin and caveolin-like sequences gathered. Additional sequences were obtained by screening NCBI's Expressed Sequence Tags (EST) database by BLAST searches. The following genome assemblies were also screened: *Branchiostoma floridae*, *Capitella sp.*, *Ciona intestinalis*, *Daphnia pulex*, *Helobdella robusta*, *Lottia gigantea*, *Monosiga brevicollis*, *Nematostella vectensis*, *Trichoplax adhaerens* and *Xenopus tropicalis* (DOE JGI, http://genome.jgi-psf.org); *Ciona intestinalis*, *Ciona savignyi*, *Gasterosteus aculeatus*, *Oryzias latipes* and *Takifugu rubripes* (Ensembl, http://www.ensembl.org/index.html), *Strongylocentrotus purpuratus* (UCSC, http://genome.ucsc.edu), *Caenorhabditis* genomes (Wormbase, http://www.wormbase.org) and the insect genomes of Flybase (http://flybase.bio.indiana.edu/). For the EST and genomic searches, many query sequences from the different caveolin groups were used. Since most of the caveolin duplications preceded the emergence of vertebrates, the sequence search strategy was limited in mammals and particularly targeted the non-vertebrate metazoans to resolve this pattern of duplication. For the final dataset, all the partial sequences were discarded and to speed up the calculations, a maximum of five placental mammal sequences were kept for each group of caveolin.

Genomic localizations of caveolin genes were determined using the UCSC genome browser (Karolchik et al., 2003) BLAT search or BLAST searches of genome assemblies at Ensembl, JGI or Wormbase websites. The sequence alignment is in supplementary material Fig. S1 and the accession numbers and genomic localization in supplementary material Table S1.

The amino acid sequences from the 118 caveolins composing the final dataset were aligned using MAFFT (Katoh et al., 2002). Phylogenetic analyses were performed with four methods: Bayesian interference, maximum-likelihood, neighbour-joining (NJ) and parsimony. Parsimony analyses were conducted with PAUP*4.0b10 (Swofford, 2003), using the tree bisection-reconnection branch swapping algorithm, heuristic searches and 500 replicates. NJ analyses were performed with MEGA3.1 (Kumar et al., 2004) using a poisson correction distance with 500 replicates; to define groups we also use the interior branch test (Sitnikova, 1996). For the Bayesian interference and ML analyses the best-fitting model of protein sequence evolution was selected by PROTTEST1.4 (Abascal et al., 2005) using the Akaike Information Criterion; the model selected was the JTT+Γ+I model (WAG+Γ+I+F when the observed amino acid frequencies were considered). ML analyses were performed with PHYML2.4.4 (Guindon and Gascuel, 2003) with the JTT+Γ+I model and 500 replicates. Bayesian analyses were performed using MRBAYES3.1.2 (Ronquist and Huelsenbeck, 2003) and the GTR+Γ+I+F model. Sampling was performed with one cold chain and three heated chains, which were run for 1,000,000 generations. Three independent runs were performed and the trees were sampled every 200th generation. Graphical inspection of the runs was then performed to determine the length of the 'burnin' stage; in all three runs the first 2500 trees were discarded before a consensus tree was generated.

This work was supported by grants from the National Health and Medical Research Council of Australia (to R.G.P. and J.F.H.), the Australian Research Council (R.G.P.), the Human Frontier Science Program grant RGP0026/2007 (to R.G.P.) and grants GM038093 (to F.M.B.) and GM47897 (to D.A.B.) from the US National Institutes of Health. L.A-R. was supported by grant AI024258 to Peter Parham from the US National Institutes of Health. The Institute for Molecular Bioscience is a Special Research Centre of the Australian Research Council. Flow cytometry analysis was performed at the Queensland Brain Institute. We thank Robert Luetterforst for expert technical assistance. We are particularly grateful to Teymuras Kurzchalia, Marino Zerial, Isabel Morrow and Chris Fielding for providing constructs for these studies.

References

Abascal, F., Zardoya, R. and Posada, D. (2005). ProtTest: selection of best-fit models of protein evolution. *Bioinformatics* **21**, 2104-2105.

Altschul, S. F., Gish, W., Miller, W., Myers, E. W. and Lipman, D. J. (1990). Basic local alignment search tool. *J. Mol. Biol.* **215**, 403-410.

Betz, R. C., Schoser, B. G., Kasper, D., Ricker, K., Ramirez, A., Stein, V., Torbergsen, T., Lee, Y. A., Nothen, M. M., Wienker, T. F. et al. (2001). Mutations in CAV3 cause mechanical hyperirritability of skeletal muscle in rippling muscle disease. *Nat. Genet.* **28**, 218-219.

Breuza, L., Corby, S., Arsanto, J. P., Delgrossi, M. H., Scheiffele, P. and Le Bivic, A. (2002). The scaffolding domain of caveolin 2 is responsible for its Golgi localization in Caco-2 cells. *J. Cell Sci.* **115**, 4457-4467.

Cagliani, R., Bresolin, N., Prelle, A., Gallanti, A., Fortunato, F., Sironi, M., Ciscato, P., Fagiolari, G., Bonato, S., Galbiati, S. et al. (2003). A CAV3 microdeletion differentially affects skeletal muscle and myocardium. *Neurology* **61**, 1513-1519.

Capozza, F., Cohen, A. W., Cheung, M. W., Sotgia, F., Schubert, W., Battista, M., Lee, H., Frank, P. G. and Lisanti, M. P. (2005). Muscle-specific interaction of caveolin isoforms: differential complex formation between caveolins in fibroblastic vs. muscle cells. *Am. J. Physiol. Cell Physiol.* **288**, C677-C691.

Carozzi, A. J., Roy, S., Morrow, I. C., Pol, A., Wyse, B., Clyde-Smith, J., Prior, I. A., Nixon, S. J., Hancock, J. F. and Parton, R. G. (2002). Inhibition of lipid raft-dependent signaling by a dystrophy-associated mutant of caveolin-3. *J. Biol. Chem.* **277**, 17944-17949.

de Paula, F., Vainzof, M., Bernardino, A. L., McNally, E., Kunkel, L. M. and Zatz, M. (2001). Mutations in the caveolin-3 gene: when are they pathogenic? *Am. J. Med. Genet.* **99**, 303-307.

Dietzen, D. J., Hastings, W. R. and Lublin, D. M. (1995). Caveolin is palmitoylated on multiple cysteine residues. Palmitoylation is not necessary for localization of caveolin to caveolae. *J. Biol. Chem.* **270**, 6838-6342.

Field, M. C., Gabernet-Castello, C. and Dacks, J. B. (2007). Reconstructing the evolution of the endocytic system: insights from genomics and molecular cell biology. *Adv. Exp. Med. Biol.* **607**, 84-96.

Fielding, P. E., Chau, P., Liu, D., Spencer, T. A. and Fielding, C. J. (2004). Mechanism of platelet-derived growth factor-dependent caveolin-1 phosphorylation: relationship to sterol binding and the role of serine-80. *Biochemistry* **43**, 2578-2586.

Fra, A. M., Williamson, E., Simons, K. and Parton, R. G. (1995). De novo formation of caveolae in lymphocytes by expression of VIP21-caveolin. *Proc. Natl. Acad. Sci. USA* **92**, 8655-8659.

Frick, M., Bright, N. A., Riento, K., Bray, A., Merrified, C. and Nichols, B. J. (2007). Coassembly of flotillins induces formation of membrane microdomains, membrane curvature, and vesicle budding. *Curr. Biol.* **17**, 1151-1156.

Fujimoto, T., Kogo, H., Nomura, R. and Une, T. (2000). Isoforms of caveolin-1 and caveolar structure. *J. Cell Sci.* **113**, 3509-3517.

Galbiati, F., Volonte, D., Minetti, C., Chu, J. B. and Lisanti, M. P. (1999). Phenotypic behavior of caveolin-3 mutations that cause autosomal dominant limb girdle muscular dystrophy (LGMD-1C). Retention of LGMD-1C caveolin-3 mutants within the golgi complex. *J. Biol. Chem.* **274**, 25632-25641.

Glebov, O. O., Bright, N. A. and Nichols, B. J. (2006). Flotillin-1 defines a clathrin-independent endocytic pathway in mammalian cells. *Nat. Cell Biol.* **8**, 46-54.

Guindon, S. and Gascuel, O. (2003). A simple, fast, and accurate algorithm to estimate large phylogenies by maximum likelihood. *Syst. Biol.* **52**, 696-704.

Hayashi, K., Matsuda, S., Machida, K., Yamamoto, T., Fukuda, Y., Nimura, Y., Hayakawa, T. and Hamaguchi, M. (2001). Invasion activating caveolin-1 mutation in human scirrhous breast cancers. *Cancer Res.* **61**, 2361-2364.

Head, B. P., Patel, H. H., Tsutsumi, Y. M., Hu, Y., Mejia, T., Mora, R. C., Insel, P. A., Roth, D. M., Drummond, J. C. and Patel, P. M. (2007). Caveolin-1 expression is essential for N-methyl-D-aspartate receptor-mediated Src and extracellular signal-regulated kinase 1/2 activation and protection of primary neurons from ischemic cell death. *FASEB J.* **22**, 828-840.

Hill, M. M., Bastiani, M., Luetterforst, R., Kirkham, M., Kirkham, A., Nixon, S. J., Walser, P., Abankwa, D., Oorschot, V. M., Martin, S. et al. (2008). PTRF-cavin, a conserved cytoplasmic protein required for caveola formation and function. *Cell* **132**, 113-124.

Karolchik, D., Baertsch, R., Diekhans, M., Furey, T. S., Hinrichs, A., Lu, Y. T., Roskin, K. M., Schwartz, M., Sugnet, C. W., Thomas, D. J. et al. (2003). The UCSC genome browser database. *Nucleic Acids Res.* **31**, 51-54.

Katoh, K., Misawa, K., Kuma, K. and Miyata, T. (2002). MAFFT: a novel method for rapid multiple sequence alignment based on fast Fourier transform. *Nucleic Acids Res.* **30**, 3059-3066.

Kirkham, M., Fujita, A., Chadda, R., Nixon, S. J., Kurzchalia, T. V., Sharma, D. K., Pagano, R. E., Hancock, J. F., Mayor, S. and Parton, R. G. (2005). Ultrastructural identification of uncoated caveolin-independent early endocytic vehicles. *J. Cell Biol.* **168**, 465-476.

Koleske, A. J., Baltimore, D. and Lisanti, M. P. (1995). Reduction of caveolin and caveolae in oncogenically transformed cells. *Proc. Natl. Acad. Sci. USA* **92**, 1381-1385.

Kumar, S., Tamura, K. and Nei, M. (2004). MEGA3: integrated software for Molecular Evolutionary Genetics Analysis and sequence alignment. *Brief. Bioinformatics* **5**, 150-163.

Kurzchalia, T. V., Dupree, P., Parton, R. G., Kellner, R., Virta, H., Lehnert, M. and Simons, K. (1992). VIP21, a 21-kD membrane protein is an integral component of trans-Golgi-network-derived transport vesicles. *J. Cell Biol.* **118**, 1003-1014.

Li, H. and Papadopoulos, V. (1998). Peripheral-type benzodiazepine receptor function in cholesterol transport. Identification of a putative cholesterol recognition/interaction amino acid sequence and consensus pattern. *Endocrinology* **139**, 4991-4997.

Li, T., Sotgia, F., Vuolo, M. A., Li, M., Yang, W. C., Pestell, R. G., Sparano, J. A. and Lisanti, M. P. (2006). Caveolin-1 mutations in human breast cancer: functional association with estrogen receptor alpha-positive status. *Am. J. Pathol.* **168**, 1998-2013.

Liu, L. and Pilch, P. F. (2008). A critical role of cavin (polymerase I and transcript release factor) in caveolae formation and organization. *J. Biol. Chem.* **283**, 4314-4322.

Luetterforst, R., Stang, E., Zorzi, N., Carozzi, A., Way, M. and Parton, R. G. (1999). Molecular characterization of caveolin association with the Golgi complex: identification of a cis-Golgi targeting domain in the caveolin molecule. *J. Cell Biol.* **145**, 1443-1459.

Machleidt, T., Li, W. P., Liu, P. and Anderson, R. G. (2000). Multiple domains in caveolin-1 control its intracellular traffic. *J. Cell Biol.* **148**, 17-28.

Marheineke, K., Grunewald, S., Christie, W. and Reilander, H. (1998). Lipid composition of Spodoptera frugiperda (Sf9) and Trichoplusia ni (Tn) insect cells used for baculovirus infection. *FEBS Lett.* **441**, 49-52.

Martin, S., Driessen, K., Nixon, S. J., Zerial, M. and Parton, R. G. (2005). Regulated localization of Rab18 to lipid droplets: effects of lipolytic stimulation and inhibition of lipid droplet catabolism. *J. Biol. Chem.* **280**, 42325-42335.

McMahon, H. T. and Gallop, J. L. (2005). Membrane curvature and mechanisms of dynamic cell membrane remodelling. *Nature* **438**, 590-596.

McNally, E. M., de Sa Moreira, E., Duggan, D. J., Bonnemann, C. G., Lisanti, M. P., Lidov, H. G., Vainzof, M., Passos-Bueno, M. R., Hoffman, E. P., Zatz, M. et al. (1998). Caveolin-3 in muscular dystrophy. *Hum. Mol. Genet.* **7**, 871-877.

Minetti, C., Sotgia, F., Bruno, C., Scartezzini, P., Broda, P., Bado, M., Masetti, E., Mazzocco, M., Egeo, A., Donati, M. A. et al. (1998). Mutations in the caveolin-3 gene cause autosomal dominant limb-girdle muscular dystrophy. *Nat. Genet.* **18**, 365-368.

Monier, S., Parton, R. G., Vogel, F., Behlke, J., Henske, A. and Kurzchalia, T. V. (1995). VIP21-caveolin, a membrane protein constituent of the caveolar coat, oligomerizes in vivo and in vitro. *Mol. Biol. Cell* **6**, 911-927.

Mora, R., Bonilha, V. L., Marmorstein, A., Scherer, P. E., Brown, D., Lisanti, M. P. and Rodriguez-Boulan, E. (1999). Caveolin-2 localizes to the golgi complex but redistributes to plasma membrane, caveolae, and rafts when co-expressed with caveolin-1. *J. Biol. Chem.* **274**, 25708-25717.

Murata, M., Peranen, J., Schreiner, R., Wieland, F., Kurzchalia, T. V. and Simons, K. (1995). VIP21/caveolin is a cholesterol-binding protein. *Proc. Natl. Acad. Sci. USA* **92**, 10339-10343.

Nixon, S. J., Wegner, J., Ferguson, C., Mery, P. F., Hancock, J. F., Currie, P. D., Key, B., Westerfield, M. and Parton, R. G. (2005). Zebrafish as a model for caveolin-associated muscle disease; caveolin-3 is required for myofibril organization and muscle cell patterning. *Hum. Mol. Genet.* **14**, 1727-1743.

Orlichenko, L., Huang, B., Krueger, E. and McNiven, M. A. (2006). Epithelial growth factor-induced phosphorylation of caveolin 1 at tyrosine 14 stimulates caveolae formation in epithelial cells. *J. Biol. Chem.* **281**, 4570-4579.

Parker, S., Peterkin, H. S. and Baylis, H. A. (2007). Muscular dystrophy associated mutations in caveolin-1 induce neurotransmission and locomotion defects in Caenorhabditis elegans. *Invert. Neurosci.* **7**, 157-164.

Parton, R. G. and Simons, K. (2007). The multiple faces of caveolae. *Nat. Rev. Mol. Cell Biol.* **8**, 185-194.

Parton, R. G., Molero, J. C., Floetenmeyer, M., Green, K. M. and James, D. E. (2002). Characterization of a distinct plasma membrane macrodomain in differentiated adipocytes. *J. Biol. Chem.* **277**, 46769-46778.

Parton, R. G., Hanzal-Bayer, M. and Hancock, J. F. (2006). Biogenesis of caveolae: a structural model for caveolin-induced domain formation. *J. Cell Sci.* **119**, 787-796.

Pelkmans, L. and Zerial, M. (2005). Kinase-regulated quantal assemblies and kiss-and-run recycling of caveolae. *Nature* **436**, 128-133.

Pol, A., Martin, S., Fernandez, M. A., Ferguson, C., Carozzi, A., Luetterforst, R., Enrich, C. and Parton, R. G. (2004). Dynamic and regulated association of caveolin with lipid bodies: modulation of lipid body motility and function by a dominant negative mutant. *Mol. Biol. Cell* **15**, 99-110.

Razani, B., Park, D. S., Miyanaga, Y., Ghatpande, A., Cohen, J., Wang, X. B., Scherer, P. E., Evans, T. and Lisanti, M. P. (2002a). Molecular cloning and developmental expression of the caveolin gene family in the amphibian Xenopus laevis. *Biochemistry* **41**, 7914-7924.

Razani, B., Wang, X. B., Engelman, J. A., Battista, M., Lagaud, G., Zhang, X. L., Kneitz, B., Hou, H., Jr, Christ, G. J., Edelmann, W. et al. (2002b). Caveolin-2-deficient mice show evidence of severe pulmonary dysfunction without disruption of caveolae. *Mol. Cell. Biol.* **22**, 2329-2344.

Journal of Cell Science

Ren, X., Ostermeyer, A. G., Ramcharan, L. T., Zeng, Y., Lublin, D. M. and Brown, D. A. (2004). Conformational defects slow Golgi exit, block oligomerization, and reduce raft affinity of caveolin-1 mutant proteins. *Mol. Biol. Cell* **15**, 4556-4567.

Rietveld, A., Neutz, S., Simons, K. and Eaton, S. (1999). Association of sterol- and glycosylphosphatidylinositol-linked proteins with Drosophila raft lipid microdomains. *J. Biol. Chem.* **274**, 12049-12054.

Ronquist, F. and Huelsenbeck, J. P. (2003). MrBayes 3, Bayesian phylogenetic inference under mixed models. *Bioinformatics* **19**, 1572-1574.

Rothberg, K. G., Heuser, J. E., Donzell, W. C., Ying, Y. S., Glenney, J. R. and Anderson, R. G. (1992). Caveolin, a protein component of caveolae membrane coats. *Cell* **68**, 673-682.

Sato, K., Sato, M., Audhya, A., Oegema, K., Schweinsberg, P. and Grant, B. D. (2006). Dynamic regulation of caveolin-1 trafficking in the germ line and embryo of Caenorhabditis elegans. *Mol. Biol. Cell* **17**, 3085-3094.

Scheel, J., Srinivasan, J., Honnert, U., Henske, A. and Kurzchalia, T. V. (1999). Involvement of caveolin-1 in meiotic cell-cycle progression in Caenorhabditis elegans. *Nat. Cell Biol.* **1**, 127-129.

Scherer, P. E., Okamoto, T., Chun, M., Nishimoto, I., Lodish, H. F. and Lisanti, M. P. (1996). Identification, sequence, and expression of caveolin-2 defines a caveolin gene family. *Proc. Natl. Acad. Sci. USA* **93**, 131-135.

Sitnikova, T. (1996). Bootstrap method of interior-branch test for phylogenetic trees. *Mol. Biol. Evol.* **13**, 605-611.

Sowa, G., Pypaert, M., Fulton, D. and Sessa, W. C. (2003). The phosphorylation of caveolin-2 on serines 23 and 36 modulates caveolin-1-dependent caveolae formation. *Proc. Natl. Acad. Sci. USA* **100**, 6511-6516.

Spisni, E., Tomasi, V., Cestaro, A. and Tosatto, S. C. (2005). Structural insights into the function of human caveolin 1. *Biochem. Biophys. Res. Commun.* **338**, 1383-1390.

Stenmark, H., Parton, R. G., Steele-Mortimer, O., Lutcke, A., Gruenberg, J. and Zerial, M. (1994). Inhibition of rab5 GTPase activity stimulates membrane fusion in endocytosis. *EMBO J.* **13**, 1287-1296.

Sun, X. H., Flynn, D. C., Castranova, V., Millecchia, L. L., Beardsley, A. R. and Liu, J. (2007). Identification of a novel domain at the N terminus of caveolin-1 that controls rear polarization of the protein and caveolae formation. *J. Biol. Chem.* **282**, 7232-7241.

Swofford, D. L. (2003). *PAUP*. Phylogenetic Analysis Using Parsimony (*and Other Methods).* Sunderland, MA: Sinauer Associates.

Tang, Z., Scherer, P. E., Okamoto, T., Song, K., Chu, C., Kohtz, D. S., Nishimoto, I., Lodish, H. F. and Lisanti, M. P. (1996). Molecular cloning of caveolin-3, a novel member of the caveolin gene family expressed predominantly in muscle. *J. Biol. Chem.* **271**, 2255-2261.

Tang, Z., Okamoto, T., Boontrakulpoontawee, P., Katada, T., Otsuka, A. J. and Lisanti, M. P. (1997). Identification, sequence, and expression of an invertebrate caveolin gene family from the nematode Caenorhabditis elegans. Implications for the molecular evolution of mammalian caveolin genes. *J. Biol. Chem.* **272**, 2437-2445.

Thomsen, P., Roepstorff, K., Stahlhut, M. and van Deurs, B. (2002). Caveolae are highly immobile plasma membrane microdomains, which are not involved in constitutive endocytic trafficking. *Mol. Biol. Cell* **13**, 238-250.

Vatta, M., Ackerman, M. J., Ye, B., Makielski, J. C., Ughanze, E. E., Taylor, E. W., Tester, D. J., Balijepalli, R. C., Foell, J. D., Li, Z. et al. (2006). Mutant caveolin-3 induces persistent late sodium current and is associated with long-QT syndrome. *Circulation* **114**, 2104-2112.

Wakeham, D. E., Abi-Rached, L., Towler, M. C., Wilbur, J. D., Parham, P. and Brodsky, F. M. (2005). Clathrin heavy and light chain isoforms originated by independent mechanisms of gene duplication during chordate evolution. *Proc. Natl. Acad. Sci. USA* **102**, 7209-7214.

Way, M. and Parton, R. G. (1996). M-caveolin, a muscle-specific caveolin-related protein. *FEBS Lett.* **378**, 108-112.

Wimley, W. C. and White, S. H. (1996). Experimentally determined hydrophobicity scale for proteins at membrane interfaces. *Nat. Struct. Biol.* **3**, 842-848.

Woodman, S. E., Sotgia, F., Galbiati, F., Minetti, C. and Lisanti, M. P. (2004). Caveolinopathies: mutations in caveolin-3 cause four distinct autosomal dominant muscle diseases. *Neurology* **62**, 538-543.